


# Electroless Plating of Ni-P and Ni-P-PTFE on Micro-Arc Oxidation Coatings for Improved Tribological Performance

Zhaoxiang Chen<sup>a,b</sup>, Li Zhu<sup>a,b</sup>, Limei Ren<sup>a,c,\*</sup> , Jialin Liu<sup>a,b</sup>

<sup>a</sup>Yanshan University, School of Mechanical Engineering, Qinhuangdao 066004, China.

<sup>b</sup>Yanshan University, Aviation Key Laboratory of Science and Technology on Generic Technology of Self-lubricating Spherical Plain Bearing, Qinhuangdao 066004, China.

<sup>c</sup>Ministry of Education of China, Yanshan University, Key Laboratory of Advanced Forging & Stamping Technology and Science, Qinhuangdao 066004, China.

Received: February 25, 2022; Revised: May 01, 2022; Accepted: July 19, 2022

Although micro-arc oxidation (MAO) coatings are widely used for anti-wear protection of metals, they usually contain lots of pores and exhibit high coefficient of friction. In this work, porous MAO coatings consisting of  $Al_2TiO_5$  were fabricated on the titanium substrate, and then Ni-P and Ni-P-polytetrafluoroethylene (PTFE) were deposited via electroless plating to fill MAO pores and improve the tribological performance. Electroless deposited Ni-P has high wear resistance and the incorporated PTFE particles have self-lubricating property. Results show that the micro-pores of the MAO coating were completely filled by deposited Ni-P and Ni-P-PTFE, and the self-lubricating PTFE particles distributed uniformly in the coating. For the MAO-Ni-P-PTFE coating, the MAO and Ni-P components mechanically interlocked and played a load-carrying role during the tribological test, and the dispersed PTFE particles produced low friction. Compared with the MAO and MAO-Ni-P coatings, the MAO-Ni-P-PTFE coating exhibited much lower coefficient of friction and wear rate.

**Keywords:** *Micro-arc oxidation, electroless plating, Ni-P, PTFE, tribological performance.*

## 1. Introduction

Titanium and its alloys, because of their low density, high specific strength and good biocompatibility<sup>1-4</sup>, are attractive in many industry fields such as aerospace, automotive and medicine. Unfortunately, the tribological application of titanium alloy is seriously limited due to its low surface hardness and poor anti-wear ability. Micro-arc oxidation (MAO) of titanium alloy can form a well-adhered oxide coating on the surface with significantly enhanced surface hardness and anti-wear ability<sup>5-9</sup>. Furthermore, the MAO technology is relatively cheap, easy to handle and environmentally friendly<sup>8-10</sup>. However, continuous spark discharge and gas evolution during the MAO process result in the formation of many micro-pores and micro-projections in the coating<sup>10,11</sup>. These micro-defects in the MAO ceramic coating often lead to relatively high and unstable coefficient of friction against many counterparts, thus aggravating the wear of MAO coatings and counterpart materials<sup>12-14</sup>. Thus, how to improve the microstructure and tribological performance of MAO coatings becomes essential to broadening the application of MAO coatings. It is reported that filling the micro-pores with solid lubricants is an effective way for this purpose<sup>15</sup>. For one thing, lots of micro-pores in the MAO coating provide sufficient spaces for the storage of solid lubricants. For another, solid lubrication is more suitable for MAO coatings because they are often used in extreme conditions such as high vacuum, high temperature and

radioactive environments where liquid lubricants prone to volatilize or deteriorate<sup>16</sup>.

Solid lubricants can be filled into the micro-pores of MAO coatings via technologies such as magnetron sputtering, electrophoretic deposition and electroless plating<sup>17-21</sup>. Chen et al.<sup>17</sup> combined micro-arc oxidation and magnetron sputtering technologies to fabricate a self-lubricating MAO/DLC composite coating and resulted in significantly decreased coefficient of friction compared with the single MAO coating. However, magnetron sputtering technology was difficult to achieve conformal growth of solid lubricants in the complex micro-pores of the MAO coating due to the directional nature of this method. As a result, solid lubricants were usually deposited on the coating surface instead of entering deep into the pores, leading to a short-time lubrication effect. Ma et al.<sup>18</sup> adopted the electrophoretic deposition technology to fabricate a MAO/MoS<sub>2</sub> composite coating and reduced the coefficient of friction by 35%. For the electrophoretic deposition technology, gravity sedimentation of solid particles and low electrical conductivity of MAO coatings are adverse factors affecting the incorporation efficiency of solid lubricants into the MAO coating<sup>19</sup>.

Currently, electroless nickel-phosphorous (Ni-P) plating technology is gaining more and more attention due to its remarkable advantages<sup>20</sup>. First, electroless plating is particular suitable for the workpieces with complex shape and deep pores because the plating solution can easily infiltrate into irregular deep pores<sup>21,22</sup>. In addition, through proper sensitization and activation pretreatment, electroless plating

\*e-mail: [lmren@ysu.edu.cn](mailto:lmren@ysu.edu.cn)

can be performed on non-metallic surfaces<sup>20-22</sup>. Another important advantage of the electroless plating technology is the co-deposition of functional particles together with Ni-P coatings<sup>23,24</sup>. Studies have shown that the introduction of solid lubricant particles (e.g., MoS<sub>2</sub>, graphite, BN, carbon nanotube, polytetrafluoroethylene (PTFE), etc.) into the electroless Ni-P coating can further improve the tribological performance of the composite coating<sup>25-29</sup>. Hu et al.<sup>25</sup> added nano-MoS<sub>2</sub> particles into the plating solution and successfully prepared a Ni-P-(nano-MoS<sub>2</sub>) composite coating with a coefficient of friction of only 0.25. Yang et al.<sup>26</sup> investigated the tribological behavior of Ni-P-(single-walled carbon nanotubes, SWCNTs) composite coating deposited by electroless plating. It was found that the Ni-P-SWCNTs composite coating showed not only higher wear resistance but also lower coefficient of friction than the Ni-P coating. PTFE particles have low coefficient of friction and high chemical stability, rendering them very suitable for the co-deposition with Ni-P<sup>27-29</sup>. Wu et al.<sup>29</sup> prepared an electroless Ni-P-PTFE composite coating on mild carbon steel and studied its tribological properties. The results showed that the average coefficient of friction of the coating decreased from 0.33 to 0.12 with the increasing PTFE content from 4.2 to 15.2 wt. %. However, it is worth noting that the electroless Ni-P-PTFE coating had weak adhesion to the steel substrate when the PTFE content was high, which caused severe coating delamination during the tribological test<sup>29</sup>.

As analyzed above, the porous MAO coatings have good adhesion to the metal substrate but exhibit high coefficient of friction, while the electroless Ni-P-PTFE coatings possess low coefficient of friction but lack strong adhesion to the metal substrate. Therefore, it may be a viable option to fabricate a MAO-Ni-P-PTFE composite coating with better tribological performance by using micro-arc oxidation in combination with electroless plating technique. To the best of our knowledge, there is no report on the preparation of MAO-Ni-P-PTFE composite coating on the titanium substrate. Therefore, in this work, Ni-P and Ni-P-PTFE were deposited on MAO coatings via electroless plating to fill MAO pores and improve the tribological performance. The microstructure and tribological properties of the fabricated MAO-Ni-P and MAO-Ni-P-PTFE coatings were investigated using scanning electron microscopy (SEM), energy-dispersive X-ray spectroscopy (EDS), micro-hardness tester and ball-on-plate tribometer test, and then compared with the single MAO coating.

## 2. Materials and Methods

### 2.1. Fabrication of MAO coatings

The commercially pure titanium (30 mm × 25 mm × 3 mm) was used as the substrate for preparing the MAO coating. The chemical composition (wt. %) of the titanium substrate was Fe ≤ 0.30, Si ≤ 0.15, C ≤ 0.10, N ≤ 0.03 and

Ti balance. Prior to the MAO process, the substrate surface was successively ground using a series of SiC abrasive papers with three grades of 150, 600, and 1200-grit and then ultrasonically cleaned in an alcoholic solution for 30 min and blow-dried for later use. A pulsed asymmetric bipolar AC power supply (MAO120HD-III, Xi'an University of Technology, China) was employed for the MAO process. The micro-arc oxidation of titanium was carried out under the mode of constant voltage and the electrical parameters setting is listed in Table 1. A dilute alkaline electrolyte consisting of 10 g/L NaAlO<sub>2</sub> and 2 g/L NaOH was used, and the titanium sample and two stainless steel plates served as the anode and cathode, respectively. A circulating cooling system was used to keep the electrolyte temperature below 40 °C. The fabricated MAO coating samples were cleaned with deionized water and dried at ambient temperature.

### 2.2. Fabrication of MAO-Ni-P and MAO-Ni-P-PTFE coatings

The MAO coating belongs to the hard-to-plate substrates and it needs to be activated before the electroless plating. In this study, the MAO coating samples were immersed in a solution consisting of 40 ml/L HF and 50 ml/L HCl for 6 s to activate them. After the activation, the MAO coating samples were rinsed with deionized water, and then transferred into the electroless plating solution for the plating at 85 °C. The solution composition used for the plating of Ni-P and Ni-P-PTFE is presented in Table 2 and the solution pH value was 4.5. The electroless plating time for the Ni-P and the Ni-P-PTFE was set to 2.5 and 5 h respectively. During the plating process, a magnetic stirrer was used to circulate the plating solution to alleviate the agglomeration and gravity sedimentation of PTFE particles. After the electroless plating, the coating samples were rinsed with deionized water and blown dry. Figure 1 illustrates schematic diagram of the preparation process of the MAO-Ni-P and MAO-Ni-P-PTFE coatings on the titanium substrate.

### 2.3. Characterization and tribological test of coatings

The surface and cross-sectional morphologies of coatings were observed by using scanning electron microscopy (SEM, SIGMA-500, ZEISS, Jena, Germany) equipped with energy dispersive spectroscopy (EDS). The phase composition of coatings was characterized by using an X-ray diffractometer (XRD, D/MAX 2500/PC, Rigaku, Japan). The XRD measurement was carried out in the 2θ range of 10-80°, at a scanning speed of 2°/min, and with a grazing incidence angle of 2°. The hardness of coatings was measured by using a micro-hardness tester (FUTURE-TECH FM-ARS 9000, Japan) at an applied load of 10 gf for 15 s. The measurement was performed on the coating surface using a diamond square-based pyramid indenter. Reported values were averaged from 5 measurements.

**Table 1.** The parameters setting of micro-arc oxidation power supply.

Parameter	Voltage (V)	Frequency (Hz)	Duty Ratio (%)	Processing Time (min)
Forward	500	400	25	20
Reverse	50	300	15	

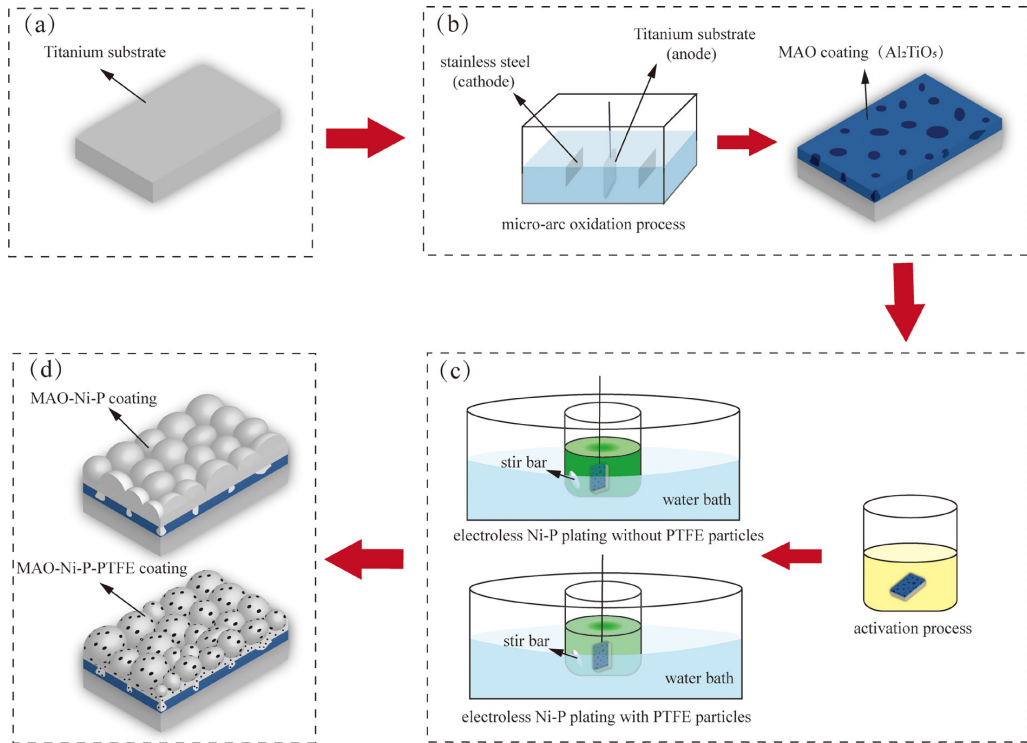


**Figure 1.** Schematic diagram of the preparation of the MAO-Ni-P and MAO-Ni-P-PTFE coatings.

**Table 2.** The solution composition used for the plating of Ni-P and Ni-P-PTFE.

Chemicals	Concentrations	
	Ni-P	Ni-P-PTFE
$\text{NiSO}_4 \cdot 6\text{H}_2\text{O}$ (g/L)	25	25
$\text{NaH}_2\text{PO}_2 \cdot \text{H}_2\text{O}$ (g/L)	30	30
$\text{CH}_3\text{COONa} \cdot 3\text{H}_2\text{O}$ (g/L)	15	15
$\text{Na}_3\text{C}_6\text{H}_5\text{O}_7 \cdot 2\text{H}_2\text{O}$ (g/L)	10	10
Lactic acid (ml/L)	20	20
60% PTFE suspension (ml/L)	-	10
FC-134 (g/L)	-	0.1

The tribological properties of as-deposited coatings were measured at room temperature under dry sliding condition by using a ball-on-plate reciprocating tribometer (MS-M9000, Lanzhou Huahui Instrument Technology Co., Ltd., China). The GCr15 stainless steel ball, with a diameter of 6 mm, was used as the grinding counterpart. The tribo-tests were carried out under a normal load of 5 N with a sliding distance of 100 m and a sliding velocity of 10 cm/s. Triplicate tests were carried out for each coating sample to ensure repeatability. After the tests, the wear tracks were measured by a surface profiler (Marsurf, Mahr, Göttingen, Germany). The reference line used to calculate the depth of the wear track corresponded to the mean line of the roughness profile of the coating around the track. The wear rate of samples was calculated according to the formula<sup>30</sup>:  $K=(S \cdot l)/(F \cdot L)$ , where S is the cross-sectional area of wear track ( $\text{mm}^2$ ), l is the length of the wear track (mm), F is the applied load (N), L is the sliding distance (m).

## 3. Results and Discussion

### 3.1. Microstructure, composition and hardness of coatings

Figure 2 shows XRD patterns of MAO, MAO-Ni-P and MAO-Ni-P-PTFE coatings. It can be found from Figure 2a that the MAO coating was mainly made up of  $\text{Al}_2\text{TiO}_5$  phase. The XRD diffraction peaks corresponding to the titanium substrate cannot be detected due to the masking effect of thick MAO coatings. XRD patterns of MAO-Ni-P and MAO-Ni-P-PTFE coatings are shown in Figure 2b and c respectively. These two XRD patterns both had a significant and broad diffraction peak at  $2\theta = 45^\circ$ , which corresponded to the deposited Ni-P materials. The broadening of this peak was due to the distortion of the crystal lattice of nickel by phosphorus atom and some degree of amorphization<sup>31,32</sup>. Also, it can be noted from Figure 2b that the characteristic peaks of the MAO coating have disappeared after the electroless deposition of Ni-P layer, implying that the deposited Ni-P layer had a good sealing effect on the underneath MAO layer. The XRD pattern shown in Figure 2c proved the existence of PTFE particles in the Ni-P layer with the characteristic diffraction peak of PTFE appearing at  $2\theta = 18^\circ$ . Besides, the characteristic peaks of  $\text{Al}_2\text{TiO}_5$  phase can be detected by X-ray for the MAO-Ni-P-PTFE coating, which indicates that adding PTFE particles to the plating solution decreased the compactness of the deposited Ni-P layer. The relatively porous Ni-P-PTFE surface layer allowed the X-ray to penetrate through it and reach the underneath MAO layer.

The surface morphology of the MAO coating produced in this work is illustrated in Figure 3a. It can be seen that



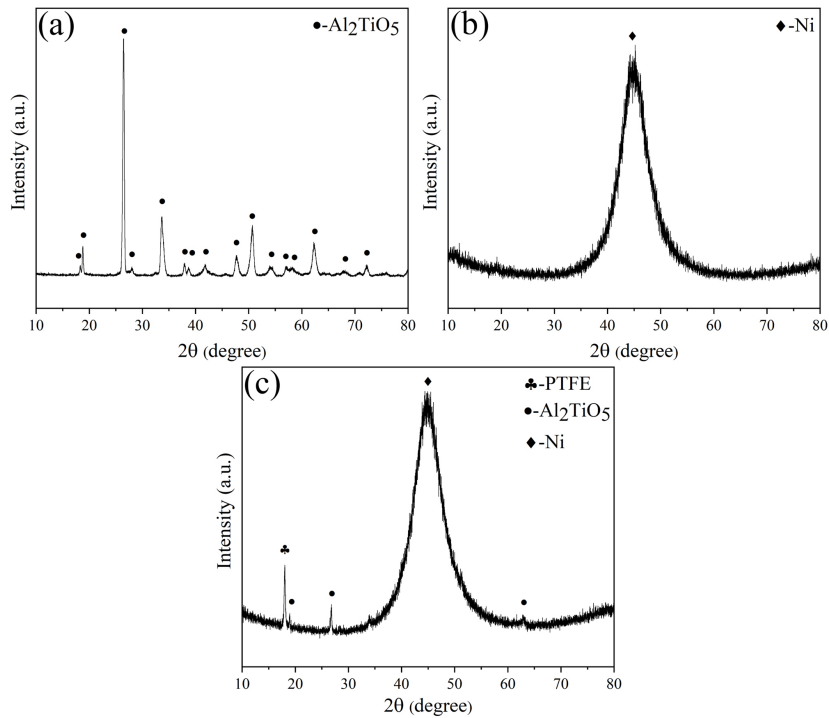


**Figure 2.** XRD patterns of MAO (a), MAO-Ni-P (b) and MAO-Ni-P-PTFE (c) coatings.

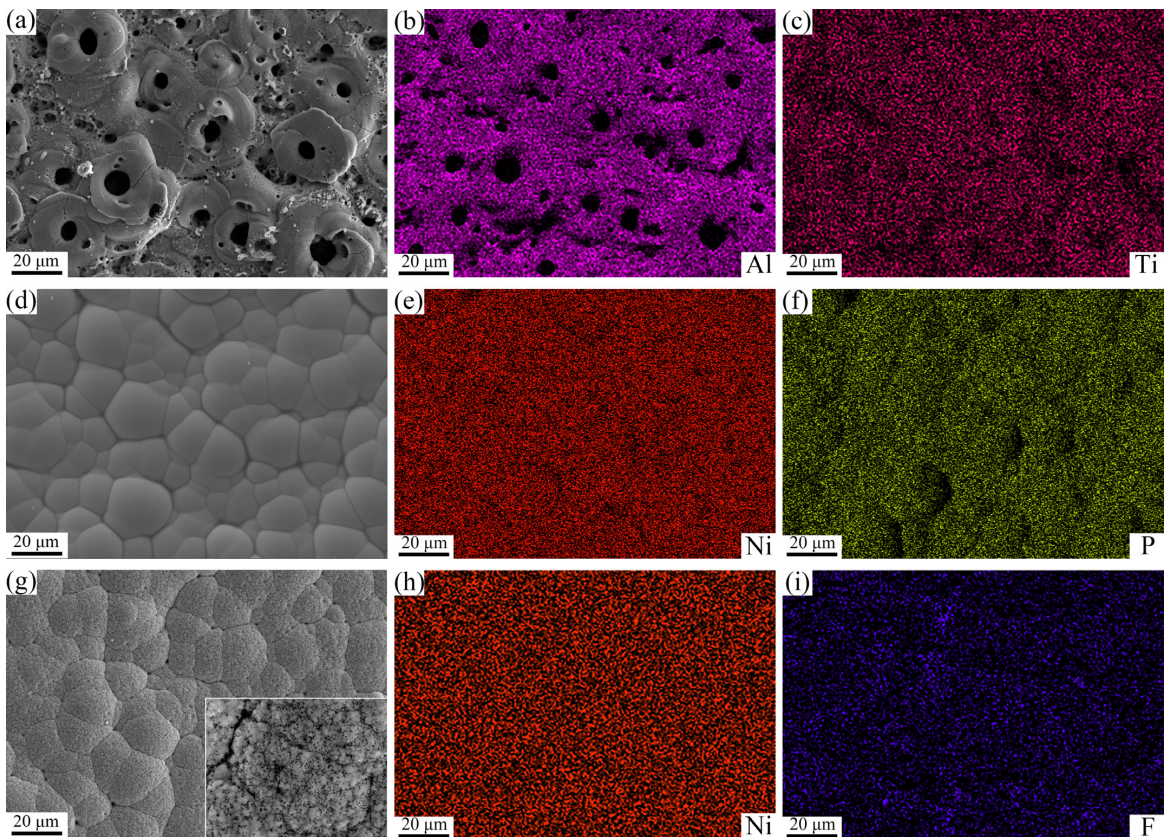


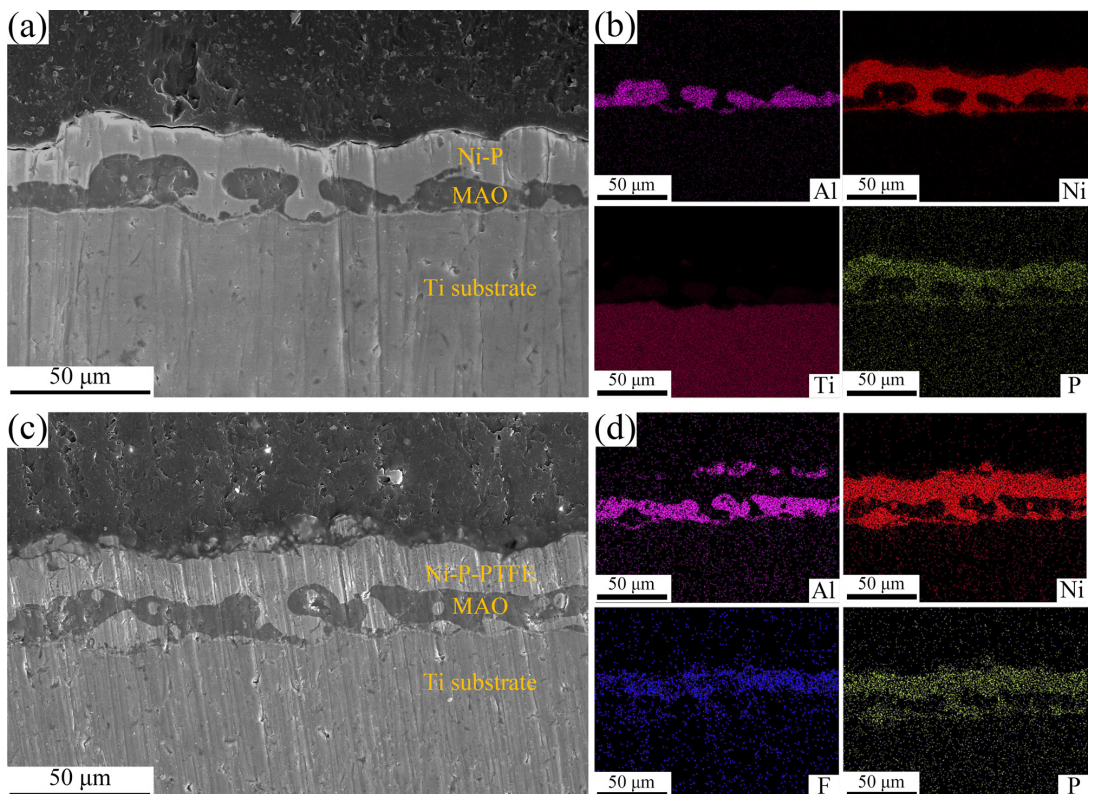
**Figure 3.** Surface morphologies and corresponding EDS element maps of MAO (a, b, c), MAO-Ni-P (d, e, f) and MAO-Ni-P-PTFE (g, h, i) coatings. The inset in g is the high magnification morphology of the MAO-Ni-P-PTFE coating. The fluorine in i indicated the position of the fluorine-based polymer PTFE.

the MAO coating comprised many crater-like micro-pores and a few micro-cracks. They were formed under the action of intense spark discharge, gas overflow and thermal stress during the micro-arc oxidation process<sup>11</sup>. The existence of these micro-defects makes it possible for Ni-P materials and PTFE particles to be stored in the MAO coating. Al and Ti elements were detected on the MAO coating surface, as displayed in the corresponding elemental maps (Figure 3b and c), revealing the formation of  $Al_2TiO_5$ . This result is consistent with the XRD pattern shown in Figure 2a. The surface morphology of the MAO-Ni-P coating is shown in Figure 3d. It can be found that the original porous surface of the MAO coating has been totally replaced by a nodular surface, a typical morphology of Ni-P coating that was formed by electroless plating<sup>33</sup>. Together with the corresponding Ni and P elemental maps and the XRD results shown in Figure 2b, it can be concluded that Ni-P coating was successfully deposited on the MAO surface and the MAO pores have been sealed completely. Similar to the MAO-Ni-P coating, the MAO-Ni-P-PTFE coating also exhibited a nodular surface morphology, as shown in Figure 3g. But unlike the smooth spherical nodules on the MAO-Ni-P coating, the spherical nodules on the MAO-Ni-P-PTFE coating had a pitted surface and were dotted with particles, as shown in the inset in Figure 3g. These particles corresponded to PTFE co-deposited along with Ni-P during the plating process, as demonstrated by the corresponding Ni and F elemental maps and the XRD pattern shown in Figure 2c. In addition, it should be pointed out that the addition of PTFE particles in the Ni-P plating solution affected the deposition efficiency and the uniformity of Ni-P

layer. Compared with the Ni-P layer, the Ni-P-PTFE layer took longer deposition time to achieve the same thickness.

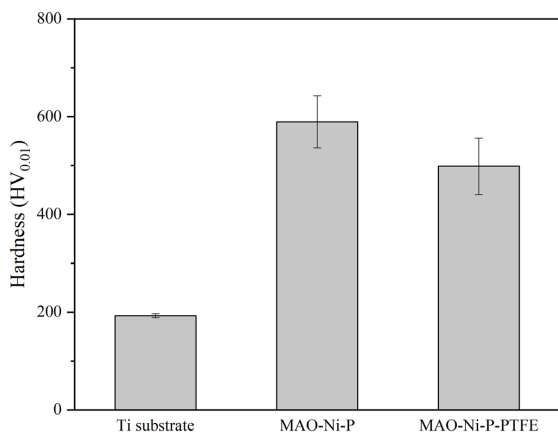
In order to achieve good pore-filling effect, Ni-P or Ni-P-PTFE should deposit not only on the MAO surface, but also in the MAO pores. The cross-sectional morphologies and corresponding elemental maps of the MAO-Ni-P and MAO-Ni-P-PTFE coatings are shown in Figure 4. It can be seen from Figure 4a that the fabricated MAO-Ni-P coating consisted of the Ni-P surface layer and the underneath MAO layer. The Ni-P materials have filled the micro-pores of the MAO layer completely and a good mechanical interlocking was formed between them. Similarly, the Ni-P-PTFE materials also infiltrated into the MAO layer, as shown in Figure 4c and d. Furthermore, the distribution of F element was consistent with that of Ni and P elements, indicating that the incorporation of PTFE particles took place synchronously with the deposition of Ni-P layer. The uniform distribution of PTFE particles along the cross section of the composite coating guaranteed the continuous lubrication performance, as will be seen in the following section. In addition, Al element can also be observed on top of the Ni-P-PTFE layer, as shown in Figure 4d. This is because some  $Al_2TiO_5$  debris was trapped in the gap between the Ni-P-PTFE layer and the epoxy resin during the preparation of the coating sample for the observation of cross-sectional morphology.

Figure 5 shows the hardness of the titanium substrate, Ni-P layer of the MAO-Ni-P coating and Ni-P-PTFE layer of the MAO-Ni-P-PTFE coating. It can be seen from Figure 5 that the hardness of Ni-P layer of the MAO-Ni-P coating was about three times that of the titanium substrate.



**Figure 4.** Cross-sectional morphologies and corresponding EDS elemental maps of MAO-Ni-P (a, b) and MAO-Ni-P-PTFE (c, d) coatings.





**Figure 5.** Hardness of Ti substrate, Ni-P layer of the MAO-Ni-P coating and Ni-P-PTFE layer of the MAO-Ni-P-PTFE coating.

The high coating hardness is crucial for improving the wear resistance of the titanium substrate. Although the hardness of Ni-P-PTFE layer of the MAO-Ni-P-PTFE coating decreased slightly due to the incorporation of soft PTFE particles, it was still much higher than that of the titanium substrate.

### 3.2. Tribological performance of coatings

Friction and wear tests were carried out to investigate the tribological performance of the MAO coating before and after the electroless plating of Ni-P and Ni-P-PTFE. Dry sliding tests of coatings were conducted at ambient temperature under the normal load of 5 N with the GCr15 ball as the counterpart. Figure 6 exhibits the curves of coefficient of friction of MAO, MAO-Ni-P and MAO-Ni-P-PTFE coatings. It can be seen that the coefficient of friction of the MAO coating showed an upward trend before the sliding distance of about 15 m, and then gradually decreased and stabilized at about 0.55. The reason for this phenomenon is related to the unique microstructure of the MAO coating. Previous studies have shown that the MAO coating consists of a porous outer layer with many micro-protrusions and a dense inner layer well bonded to the substrate<sup>12</sup>. At the beginning of the friction test, the GCr15 counterpart contacted with the porous outer layer of the MAO coating and the surface micro-protrusions impeded the relative motion between them, resulting in a high coefficient of friction up to about 0.68. With the proceeding of the friction test, the micro-protrusions gradually fractured under the action of shear force and the formed wear debris filled into the micro-pores of the outer layer, which increased the contact area between the friction pair. Besides, with the gradual worn-off of the porous outer layer, the counterpart ball began to contact with the denser inner layer of the MAO coating. As a result, the coefficient of friction began to decline and reached a plateau.

In contrast, the MAO-Ni-P coating exhibited a much lower and relatively steadier coefficient of friction compared with the MAO coating. This behavior is attributed to the dense and uniform structure of the MAO-Ni-P composite coating. As mentioned above, the Ni-P in situ grew both on the MAO surface and in the MAO pores during the electroless plating. The deposited Ni-P layer covered the MAO micro-protrusions and filled the MAO pores completely,

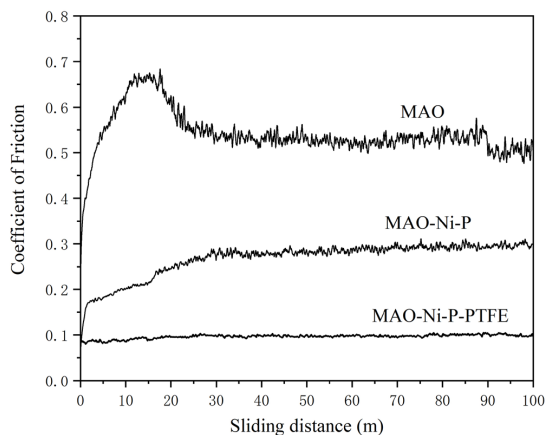


**Figure 6.** Curves of coefficient of friction of MAO, MAO-Ni-P and MAO-Ni-P-PTFE coatings.

and thus avoided the direct contact of the counterpart ball with the porous and rough MAO coating, thereby resulting in a decreased and stable coefficient of friction. Compared with the MAO and MAO-Ni-P coatings, the coefficient of friction of the MAO-Ni-P-PTFE coating was significantly reduced to about 0.09, and the curve of coefficient of friction remained in a steady state with small fluctuation throughout the friction test. Considering that the major difference between the MAO-Ni-P and the MAO-Ni-P-PTFE coatings lied in that the latter contained lots of PTFE particles, it is reasonable to believe that the incorporated PTFE particles functioned as solid lubricants and played a lubricating role during the tribo-test.

Figure 7 exhibits the SEM images and cross-sectional profiles of wear tracks of MAO, MAO-Ni-P and MAO-Ni-P-PTFE coatings after a sliding distance of 100 m under the load of 5 N. Comparing the wear tracks of MAO and MAO-Ni-P coatings, it can be observed that these two coatings had similar wear depth but different wear width. To be specific, the wear width of the MAO coating (~1118  $\mu\text{m}$ ) was about 2.5 times that of the MAO-Ni-P coating (~443  $\mu\text{m}$ ). This phenomenon was caused by two reasons. First, the MAO ceramic coating was more prone to fragment and detach than the MAO-Ni-P coating due to its porous surface structure and high brittleness. Secondly, the MAO coating caused higher wear of the counterpart ball than the MAO-Ni-P coating because the hardness of the MAO coating (~894 HV) was higher than that of the GCr15 counterpart (~697 HV) and the Ni-P layer of the MAO-Ni-P coating (~589 HV)<sup>5,7</sup>. Comparing the wear tracks of MAO-Ni-P and MAO-Ni-P-PTFE coatings, it can be noted that both the wear width (~366  $\mu\text{m}$ ) and wear depth (~8  $\mu\text{m}$ ) of the MAO-Ni-P-PTFE coating was smaller than that of the MAO-Ni-P coating. This indicated that the introduction of self-lubricating PTFE particles into the MAO-Ni-P coating significantly mitigated the wear between the MAO-Ni-P coating and the GCr15 counterpart ball.

Figure 8 shows the worn morphologies and corresponding elemental maps of MAO, MAO-Ni-P and MAO-Ni-P-PTFE coatings. It can be noticed that the MAO coating had two kinds of typical worn morphologies, as shown in Figure 8a. The worn morphology on the left area of Figure 8a was relatively

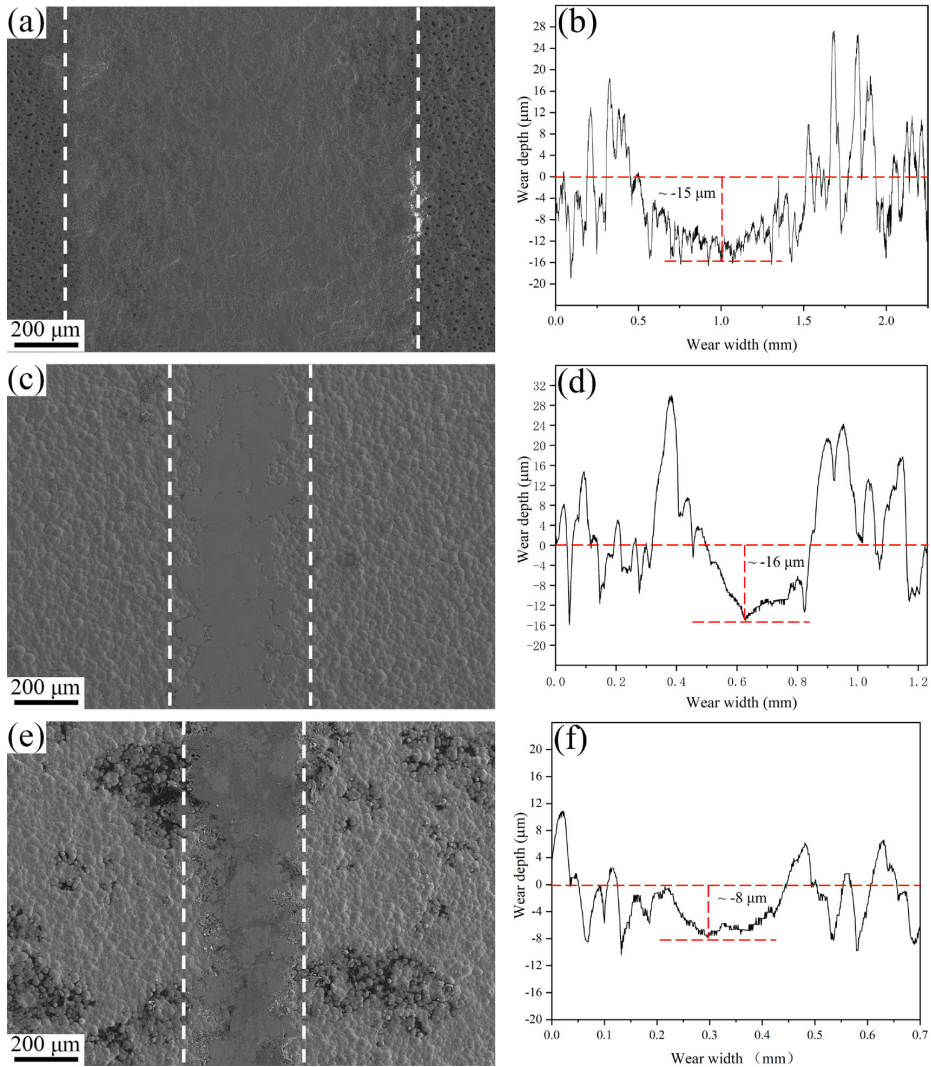


**Figure 7.** SEM images and cross-sectional profiles of wear tracks of MAO (a, b), MAO-Ni-P (c, d) and MAO-Ni-P-PTFE (e, f) coatings.

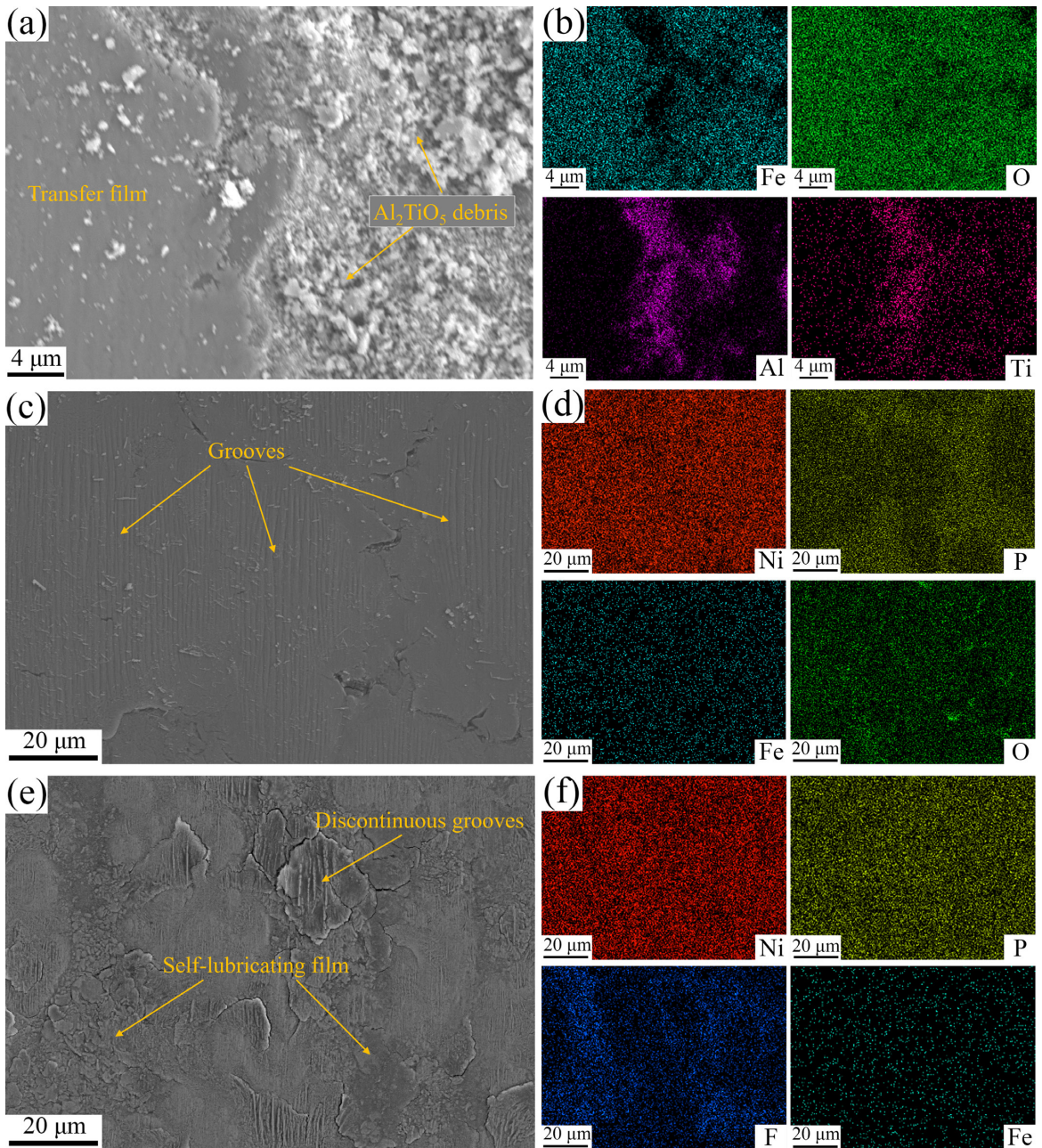
smooth and lots of Fe and O elements were detected there (see the corresponding elemental maps shown in Figure 8b), indicating that this area was the transfer film consisting mainly of Fe transferred from the GCr15 ball and its oxides. The worn morphology on the right area of Figure 8a was relatively rough and rich in Al and Ti elements, indicating the existence of MAO coating and detached  $\text{Al}_2\text{TiO}_5$  debris there. As mentioned above, there were micro-pores in the surface layer of the MAO coating, which promoted the crack initiation. The initiated cracks propagated in the MAO coating under the repeated action of friction and caused the spallation and detachment of MAO porous layer.

Figure 8c shows the worn surface morphology of the MAO-Ni-P coating. It can be found that this worn surface was relatively smooth and contained rows of longitudinal grooves. The presence of grooves demonstrated the micro-cutting and micro-ploughing effect of the harder GCr15 counterpart ball. This phenomenon is reasonable because the hardness of Ni-P layer of the MAO-Ni-P coating ( $\sim 589$  HV) was smaller than that of the GCr15 counterpart

( $\sim 697$  HV). The EDS analysis of the worn surface shown in Figure 8d revealed lots of Ni and P elements and few Fe element, indicating that the MAO-Ni-P coating suffered from significant abrasive wear and few Fe was transferred to the coating surface during the tribo-test.

Compared with the MAO-Ni-P coating, the worn surface of the MAO-Ni-P-PTFE coating was relatively rough, and the longitudinal grooves became discontinuous and even disappeared in many areas, as shown in Figure 8e. This means that the MAO-Ni-P-PTFE coating suffered from less abrasive wear than the MAO-Ni-P coating. In addition to Ni and P elements, abundant F element was also present on the worn surface (see the elemental maps shown in Figure 8f), indicating the formation of self-lubricating PTFE film. During the friction and wear test, PTFE particles incorporated in the composite coating were gradually exposed with the proceeding of friction test and then these particles cross-linked with each other to form a continuous PTFE film on the coating surface. This formed PTFE film effectively separated the composite coating from





**Figure 8.** Worn morphologies and corresponding elemental maps of MAO (a, b), MAO-Ni-P (c, d) and MAO-Ni-P-PTFE (e, f) coatings.

the GCr15 counterpart during the test, thereby avoiding the direct contact of them and mitigating the abrasive wear of the coating.

Figure 9 shows the wear rates of three kinds of coatings against the GCr15 counterpart ball after a sliding distance of 100 m under the load of 5 N. The wear rates of MAO and MAO-Ni-P coatings were  $8.99$  and  $3.56 \times 10^{-5} \text{ mm}^3 \cdot \text{N}^{-1} \cdot \text{m}^{-1}$ , respectively. These results indicate that the wear rate of the MAO-Ni-P coating was much lower than that of the MAO coating. This is because although these two coatings had similar wear depth, the width of the wear track of the

MAO coating was much larger than that of the MAO-Ni-P coating, as shown in Figure 7. It can also be seen that the wear rate of the self-lubricating MAP-Ni-P-PTFE coating was  $1.98 \times 10^{-5} \text{ mm}^3 \cdot \text{N}^{-1} \cdot \text{m}^{-1}$  and the smallest among three coating samples. This can be attributed to the synergistic action of the self-lubricating PTFE and the wear-resistant MAO-Ni-P. During the friction and wear test, the MAO-Ni-P played a role in bearing most of the normal load, and the self-lubricating PTFE decreased the shear stress exerting on the friction pairs and thus alleviated the abrasive wear between them.



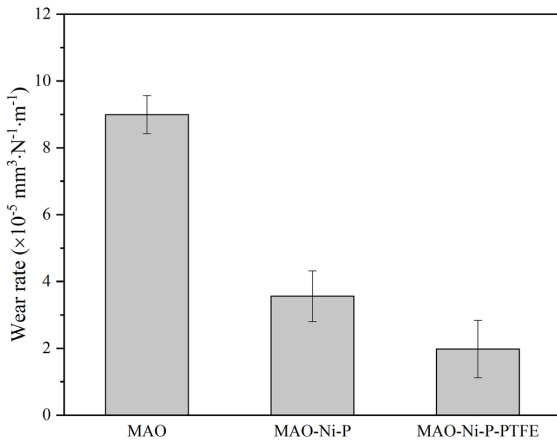


**Figure 9.** Wear rates of MAO, MAO-Ni-P and MAO-Ni-P-PTFE coatings.

#### 4. Conclusions

Porous micro-arc oxidation coatings consisting of  $\text{Al}_2\text{TiO}_5$  were fabricated on the titanium substrate, and then Ni-P and Ni-P-PTFE were deposited via electroless plating to fill MAO pores and fabricate the MAO-Ni-P and MAO-Ni-P-PTFE composite coatings. The microstructure and tribological performance of the fabricated composite coatings were investigated and compared with the single MAO coating, and the main research findings are summarized as follows:

- (1) The micro-pores of the MAO coating were completely filled by Ni-P and Ni-P-PTFE after the electroless deposition, and the deposited Ni-P mechanically interlocked with the MAO coating. The self-lubricating PTFE particles distributed uniformly in the fabricated MAO-Ni-P-PTFE coating.
- (2) Compared with the MAO and MAO-Ni-P coatings, the MAO-Ni-P-PTFE coating exhibited much lower coefficient of friction and wear rate when sliding against the GCr15 counterpart due to the synergistic action of the self-lubricating PTFE and the wear-resistant MAO-Ni-P.
- (3) During the friction and wear test of the MAO-Ni-P-PTFE coating, the MAO-Ni-P component bore most of the normal load, and the PTFE component decreased the friction as well as alleviated the abrasive wear between the coating and the GCr15 counterpart with the formation of a continuous PTFE film on the coating surface.

#### 5. Acknowledgements

This work is supported by the Natural Science Foundation of Hebei Province (E2020203057), Foundation for Science and Technology Research in Universities of Hebei Province (QN2019013) and Fundamental Research Foundation of Yanshan University (020000904).

#### 6. References

- Bai HQ, Zhong LS, Kang L, Liu JB, Zhuang WJ, Lv ZL, et al. A review on wear-resistant coating with high hardness and high toughness on the surface of titanium alloy. *J Alloys Compd.* 2021;882:160645.
- Singh P, Pungotra H, Kalsi NS. On the characteristics of titanium alloys for the aircraft applications. *Mater Today Proc.* 2017;4:8971-82.
- Boyer RR. Attributes, characteristics, and applications of titanium and its alloys. *JOM.* 2010;62(5):21-4.
- Yavari SA, van der Stok J, Chai YC, Wauthle R, Birgani ZT, Habibovic P, et al. Bone regeneration performance of surface-treated porous titanium. *Biomater.* 2014;35:6172-81.
- Chai C, Wang HY, Chen ZX, Li YY, Gao S. Friction and wear behaviors of titanium micro-arc oxidation coatings under different friction conditions. *Surf Technol.* 2021;50(7):266-75.
- Sharifi H, Aliofkhaezai M, Darband GB. A review on adhesion strength of PEO coatings by scratch test method. *Surf Rev Lett.* 2018;25(7):1830004.
- Wang HY, Li YY, Chen ZX, Chai C, Gao S. Preparation process and wear resistance optimization of titanium micro-arc oxidation film. *J Yanshan Univ.* 2021;45(6):496-504.
- Habazaki H, Tsunekawa S, Tsuji E, Nakayama T. Formation and characterization of wear-resistant PEO coatings formed on  $\beta$ -titanium alloy at different electrolyte temperatures. *Appl Surf Sci.* 2012;259:711-8.
- Ren LM, Wang TC, Chen ZX, Ren XP, Qi XW. Microstructure and tribological properties of micro-arc oxidation  $\text{TiO}_2$  coating before and after SiC particles incorporation. *Mater Sci.* 2019;25(3):270-5.
- Fan XZ, Wang Y, Zou BL, Gu LJ, Huang WZ, Cao XQ. Preparation and corrosion resistance of MAO/Ni-P composite coat on Mg alloy. *Appl Surf Sci.* 2013;277:272-80.
- Zhou R, Wei DQ, Yang HY, Cheng S, Feng W, Li BQ, et al. Osseointegration of bioactive microarc oxidized amorphous phase/ $\text{TiO}_2$  nanocrystals composited coatings on titanium after implantation into rabbit tibia. *J Mater Sci Mater Med.* 2014;25:1307-18.
- Wang SX, Zhao Q, Liu DX, Du N. Microstructure and elevated temperature tribological behavior of  $\text{TiO}_2/\text{Al}_2\text{O}_3$  composite ceramic coating formed by microarc oxidation of Ti6Al4V alloy. *Surf Coat Tech.* 2015;272:343-9.
- Zhang RZ, Han LP, Tang MQ, Ren YY, Li LJ. Research progress of micro-arc oxidation ceramic coatings and composite coatings on titanium alloy. *J Synth Cryst.* 2018;40(1):219-30.
- Li H, Sun YZ, Zhang J. Effect of  $\text{ZrO}_2$  particle on the performance of micro-arc oxidation coatings on Ti6Al4V. *Appl Surf Sci.* 2015;342:183-90.
- Lv XY, Zou GP, Ling K, Yang WW, Mo QF, Li WZ. Tribological properties of MAO/ $\text{MoS}_2$  self-lubricating composite coating by microarc oxidation and hydrothermal reaction. *Surf Coat Tech.* 2021;406:126630.
- Aliofkhaezai M, Macdonald DD, Matykina E, Parfenov EV, Egorokin VS, Curran JA, et al. Review of plasma electrolytic oxidation of titanium substrates: mechanism, properties, applications and limitations. *Appl Surf Sci Adv.* 2021;5:100121.
- Chen ZX, Ren XP, Ren LM, Wang TC, Qi XW, Yang YL. Improving the tribological properties of spark-anodized titanium by magnetron sputtered diamond-like carbon. *Coat.* 2018;8:83.
- Ma CS, Cheng D, Zhu XH, Yan ZJ, Fu JG, Yu J, et al. Investigation of a self-lubricating coating for diesel engine pistons, as produced by combined microarc oxidation and electrophoresis. *Wear.* 2018;394-395:109-12.
- Arun S, Hariprasad S, Saikiran A, Ravisankar B, Parfenov EV, Mukaeva VR, et al. The effect of graphite particle size on the corrosion and wear behaviour of the PEO-EPD coating fabricated on commercially pure zirconium. *Surf Coat Tech.* 2019;363:301-13.
- Loto CA. Electroless nickel plating-a review. *Silicon.* 2016;8:177-86.

21. Shang W, Wu F, Jiang SQ, Wen YQ, Peng N, Jiang JQ. Effect of hydrophobicity on the corrosion resistance of microarc oxidation/self-assembly/nickel composite coatings on magnesium alloys. *J Mol Liq.* 2021;330:115606.
22. Chen CA, Jian SY, Lu CH, Lee CY, Aktuğ SL, Ger MD. Evaluation of microstructural effects on corrosion behavior of AZ31B magnesium alloy with a MAO coating and electroless Ni-P plating. *J Mater Res Technol.* 2020;9(6):13902-13.
23. Zhang WH, Cao D, Qiao YX, He Z, Wang YX, Li X, et al. Microstructure and properties of duplex Ni-P-TiO<sub>2</sub>/Ni-P nanocomposite coatings. *Mater Res.* 2019;22(Suppl. 2):e20180748.
24. Du SM, Li Z, He ZT, Ding HL, Wang XC, Zhang YZ. Effect of temperature on the friction and wear behavior of electroless Ni-P-MoS<sub>2</sub>-CaF<sub>2</sub> self-lubricating composite coatings. *Tribol Int.* 2018;128:197-203.
25. Hu XG, Jiang P, Wan JC, Xu YF, Sun XJ. Study of corrosion and friction reduction of electroless Ni-P coating with molybdenum disulfide nanoparticles. *J Coat Technol Res.* 2009;6(2):275-81.
26. Yang Z, Xu H, Li MK, Shi YL, Huang Y, Li HL. Preparation and properties of Ni/P/single-walled carbon nanotubes composite coatings by means of electroless plating. *Thin Solid Films.* 2004;466:86-91.
27. Zhang RH, Zhao J, Liang J. A novel multifunctional PTFE/PEO composite coating prepared by one-step method. *Surf Coat Tech.* 2016;299:90-5.
28. Zhang YZ, Wu YY, Sun KN, Yao M. Characterization of electroless Ni-P-PTFE composite coating. *J Mater Sci Lett.* 1998;17:119-22.
29. Wu YT, Zhong C, He MF, Liu L, Hu WB. Antifriction and wear characteristics of electrolessly-deposited Ni-P with PTFE composites. *Tribol Lett.* 2011;42:161-8.
30. Kavimani V, Prakash KS, Thankachan T. Surface characterization and specific wear rate prediction of r-GO/AZ31 composite under dry sliding wear condition. *Surf Interfaces.* 2017;6:143-53.
31. Uysal M. Electroless codeposition of Ni-P composite coatings: effects of graphene and TiO<sub>2</sub> on the morphology, corrosion, and tribological properties. *Metall Mater Trans, A Phys Metall Mater Sci.* 2019;50:2331-41.
32. Sharma A, Singh AK. Electroless Ni-P-PTFE-Al<sub>2</sub>O<sub>3</sub> dispersion nanocomposite coating for corrosion and wear resistance. *J Mater Eng Perform.* 2014;23:142-51.
33. Chen MA, Cheng N, Ou YC, Li JM. Corrosion performance of electroless Ni-P on polymer coating of MAO coated AZ31 magnesium alloy. *Surf Coat Tech.* 2013;232:726-33.